Chapter 2: REALIZATION OF INTEGRATED COMPACT ULTRA-WIDEBAND AND FREQUENCY RECONFIGURABLE ANTENNA WITH HIGH ISOLATION FOR COGNITIVE RADIO

This chapter presents the design of a compact ultra-wideband (UWB) antenna and a frequency reconfigurable antenna with high isolation for cognitive radio (CR) applications. The antenna prototype comprises a UWB antenna for sensing UWB spectrum and a frequency reconfigurable antenna for communication purposes. The proposed antenna has been designed on FR-4 substrate with a compact size of $25 \times 36 \times 1.6$ mm^3 ($0.22\lambda_0 \times 0.32\ \lambda_0 \times 0.014\lambda_0$), where λ_0 is free space wavelength at 2.7 GHz. The -10 dB impedance bandwidth is realized for UWB antenna ranges from 2.7 GHz to 10 GHz and for frequency reconfigurable antenna in two frequency bands from 4.3 GHz to 5.5 GHz and 5.1 GHz to 6.8 GHz. A T-shaped stub is integrated into the ground plane to achieve high isolation between antenna element ports and the impedance bandwidth improvement. The proposed design attains mutual coupling less than -21 dB over a communication frequency range of the frequency reconfigurable antenna and most of the UWB spectrum. The prototype has been fabricated and measured. The measurement results show that the proposed antenna is a good candidate for cognitive radio applications. *

*Parts of this chapter have been published: **Praveen Singh Rathore**, Ravi Mali, Rajkumar Jatav and Manoj Kumar Meshram, "Integrated compact UWB and frequency reconfigurable antenna with high isolation for cognitive radio," *AEU- International Journal of Electronics and Communications*, vol. 171, 154899, Nov - 2023.

2.1 Introduction

The Federal Communications Commission (FCC) allotted an unlicensed ultra-wideband spectrum from 3.1 GHz to 10.6 GHz for communication [36]. This spectrum is a finite resource, and its efficient management is crucial to meet the increasing demands for wireless communication. With emerging technology such as 5G and an increase in various communication devices, the spectrum has become increasingly congested. This congestion leads to a slower data rate and high interference between devices. The frequency spectrum is underutilized, and to alleviate spectrum congestion, emerging technology such as cognitive radio (CR), dynamic spectrum sharing was discussed in [89]. CR systems are designed to adapt and optimize their communication parameters based on real-time spectrum sensing, knowledge of the environment, and user requirements [33]. In CR, there are two user types: licensed users are principal users, and unlicensed users are secondary users. Based on hierarchical sharing of the spectrum by primary and secondary users, the CR system has two types: spectrum underlay and spectrum interweave. In hierarchical sharing, the dedicated spectrum band is allocated to primary users, and the unused idle spectrum band can be granted to unlicensed users without affecting the quality of service [90, 91]. In the underlay CR system, the same portion of the spectrum is utilized by both primary and secondary users with the power level restrictions to the secondary user within the reference power level. Whereas in an interweave CR system, the entire spectrum is scanned for an idle channel, which is not being used by primary users, and this channel is allocated to secondary users by dynamic leasing.

For an interweave case, constant spectrum monitoring is required. Therefore, a UWB antenna is used for channel sensing, and a separate frequency reconfigurable antenna is used for communication [92, 93]. While mounting these antenna elements for interweave cognitive radio, good isolation between two antenna ports, compact space, and omnidirectional radiation pattern are required [94].

In literature, various reconfigurable antennas for cognitive radio have been reported [95–98]. In interweave CR, the reconfigurable antennas are narrowband antennas that operate in single-band, dual-band, or multi-band, depending upon the states of the PIN diode switch [99], while in [77], the ultra-wideband antenna covers the entire bandwidth from 3.1 GHz to 10.6 GHz for ultra-wideband scanning. Designing a compact antenna system in a single substrate with high isolation is difficult. The compact MIMO antenna for mobile devices in UWB applications with mutual coupling less than -15 dB has been reported in [86]. However, in [79], an integrated wideband and narrowband antenna for cognitive radio was presented. The system combines a UWB antenna and a narrowband antenna into one volume with a common ground plane. The mutual coupling between the antenna elements was -10 dB for the UWB band (3.1 GHz to 10.6 GHz), except in the frequency range of 4.7 GHz to 7.3 GHz, where it was -4 dB at frequency 5.15 GHz. In [78], the maximum coupling between the two antennas was -14.8 dB and as low as -31.4 dB for different states of operations, but with the increased antenna size. Similarly, the mutual coupling between a planar integrated UWB and reconfigurable antenna was -15 dB with isolated ground [100]. The cognitive radio antenna using photoconductive switches has better mutual coupling than -20 dB between antenna ports [26]. However, the photoconductive switches require complex circuitry, and the antenna has a large profile. In [101], UWB and

communication antenna mutual coupling were -16 dB. However, to cover the various frequency bands, separate antennas with distinct ground planes were utilized.

The isolation enhancement between antenna elements in CR systems with complementary split ring resonator (CSRR), defective ground structure, parasitic elements, and neutralizing block was discussed in [45, 47]. In [47], a frequency agile miniaturized MIMO antenna has been designed. The isolation enhancement between frequency agile antennas was achieved by eight complementary split ring resonators (CSRR) etched from a plus-shaped strip located between antenna elements. The mutual coupling of -29 dB was observed at 2.4 GHz, while the minimum mutual coupling achieved was -37 dB. In [45], defective ground structure, parasitic elements, and neutralizing blocks were used to achieve the mutual coupling between antenna ports to -25 dB. However, more than one method has been used to achieve the isolation, which increases the complexity of the design. The isolation enhancement between UWB antennas through a stub with a common ground plane has been reported in [62, 71, 87, 102]. However, the meander line was introduced between UWB and narrowband antennas to achieve mutual coupling of -22 dB between all ports [103]. In [104], fractal-inspired isolation improvement with band rejection for compact UWB-MIMO antenna has been reported. The mutual coupling between antennas was -20 dB. In [51], an isolating stub and multiple electromagnetic band-gap (EBG) cells were used to obtain mutual coupling of -25 dB between UWB and NB antenna, with the cost of complexity in the design and a single frequency of operation for communication.

Most of the literature has proposed the isolation enhancement between UWB-MIMO antennas. However, it is also a requirement of high isolation between the UWB antenna and the frequency reconfigurable antenna with compact size in cognitive radio, because

the frequency reconfigurable antenna works in multiple frequency bands, which covers a large band of operation for communication, and a UWB antenna is used for sensing. Apart from this, the higher harmonics contributed by frequency reconfigurable antennas give the possibility of interference with UWB antenna. Therefore, the cognitive radio with antennas exhibiting good isolation provides a solution for interference challenges and optimizing spectrum utilization.

In this chapter, a compact UWB antenna and a frequency reconfigurable antenna with high isolation for cognitive radio are proposed. It consists of a spectrum sensing UWB antenna and a frequency reconfigurable antenna for communication. A T-shaped decoupling stub is integrated into the common partial ground plane to achieve mutual coupling of -21 dB in most of the UWB spectrum.

The schematic diagram of the proposed antenna is depicted in Figure 2.1. The frequency reconfigurable communication antenna is loaded with a PIN diode. With the help of DC biasing, this PIN diode can be turned ON (State_1) or OFF (State_2) to achieve frequency reconfigurability. The proposed low-profile antenna is designed to achieve high isolation with minimal design complexity. By combining intelligent spectrum access with effective isolation techniques, this system offers improved performance, enhanced reliability, and increased efficiency in wireless communication.

Section 2.2 discusses the design of the proposed UWB, frequency reconfigurable antenna for CR, and T-shaped stub for isolation enhancement. Section 2.3 presents simulated and measured results with a discussion. This chapter concludes in section 2.4.

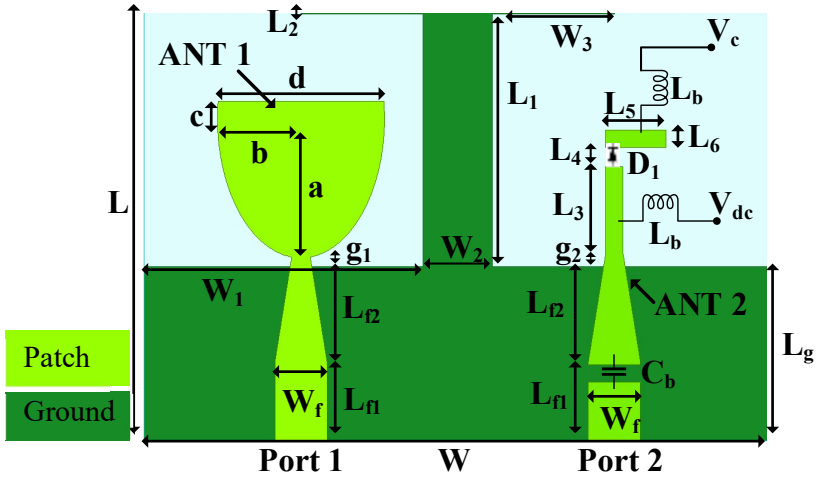

(a)

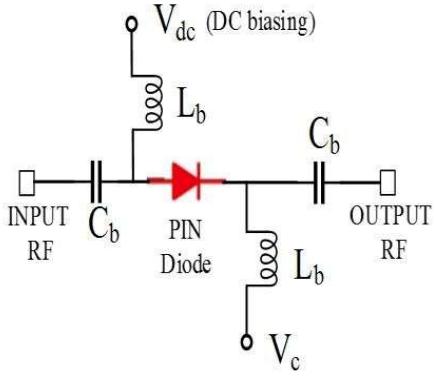

(b)

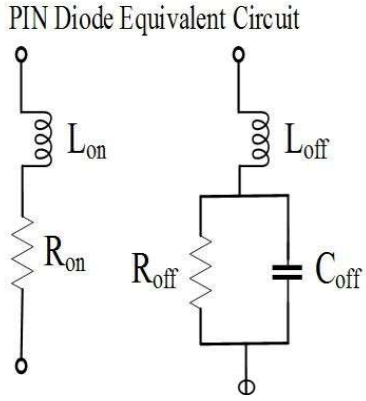

(c) (d)

Figure 2.1: (a) Proposed UWB and reconfigurable antenna with common ground plane and extended T-stub, (b) PIN diode with DC biasing, DC blocking capacitors (C_b) and RF choke (L_b), (c) PIN diode equivalent circuit in ON state, (d) PIN diode equivalent circuit in OFF state.

2.2 Antenna Design

The proposed antenna comprises an ultra-wideband antenna (ANT1) and a frequency reconfigurable monopole antenna (ANT2). Both antennas are printed on one side of the substrate (FR-4). The relative permittivity of the substrate is 4.4 with a loss tangent of 0.02, and it has a thickness of 1.6 mm. A common ground plane incorporated with a T-

shaped stub is printed on the rear side of the substrate to achieve high isolation and improved impedance bandwidth. Therefore, less space is required for this antenna. The antennas are designed as follows:

2.2.1. UWB and Frequency Reconfigurable Antenna Design

The proposed UWB antenna (ANT1) is formed by a combination of a half-ellipse and a rectangle (c × d) mm^2 [79, 105, 106, 140]. This radiator is fed with 50 Ω tapered microstrip line to achieve good impedance matching over the UWB [107]. The UWB antenna (ANT1) is separated from the frequency reconfigurable antenna (ANT2) by 18 mm (0.16 λ_0). ANT2 is a frequency reconfigurable antenna with a length of (L_3 + L_4 + L_5 + g_2) mm fed by 50 Ω tapered microstrip line. The dimensions of both radiating elements, partial ground plane, port-to-port separation, and the gap between patches and ground planes are optimized to achieve good impedance matching with high isolation.

The PIN diode (SMP1321-079LF) is used to obtain the reconfigurabilty of antenna by changing the length of (ANT2). The PIN diode has two operating states: State_1 (diode ON) and State_2 (diode OFF).

In full wave simulation, the PIN diode is modelled as a lumped RLC for different boundaries in ON and OFF states [47]. The equivalent circuit of a PIN diode is shown in Figure 2.1(b), Figure 2.1(c), and Figure 2.1(d). The PIN diode is forward-biased in State_1 (ON State), and it has very low impedance in State_1. Therefore, the PIN diode is modelled as an inductance (L_{on}) of 0.7 nH in series with a resistance (R_{on}) of 1.05 Ω. In State_2 (OFF State), it has a very high impedance. Therefore, the PIN diode is modelled as an inductance (L_{off}) of 0.7 nH in series with a capacitance (C_{off}) of 0.18 pF.

The two frequency bands of (4.3 GHz to 5.5 GHz) and (5.1 GHz to 6.8 GHz) are achieved by the reconfigurable antenna (ANT2) when it operates in State_1 and State_2, respectively. It covers the sub-6 GHz 5G (4.5 GHz), ISM bands (5.2 GHz/ 5.8 GHz), and WLAN (5/5.2/5.8 GHz) applications. In fabrication, the PIN diode (SMP1321-079LF) is biased with the help of a DC biasing voltage at nodes V_{dc} and V_c. According to the datasheet [108], the forward voltage across the diode is 0.85 volts, and the forward current is 10 mA. In State_2, the diode is in the OFF state. The DC blocking capacitor C_b blocks the DC current towards Port 2 from V_{dc}, and the RF choke L_b barricades the RF current towards V_{dc} and V_c. The optimized values of C_b and L_b are 10 pF and 18 nH, respectively. The schematic of the proposed antenna and equivalent circuit of the PIN diode with DC biasing are shown in Figure 2.1. The shape parameters of the proposed antenna are given in Table 2.1. The conditions of PIN diode states are detailed in Table 2.2.

Table 2.1: Shape parameters of proposed antenna.

Shape parameter	Value (mm)	Shape parameter	Value (mm)	Shape parameter	Value (mm)
L	25	W_f	3	a	8
W	36	L_3	5	b	4.8
L_g	10	L_4	1.1	c	1
L_1	14.5	L_5	3.45	d	9.6
L_2	0.5	L_6	1	W_1	16
L_{f1}	4.5	g_1	0.5	W_2	4
L_{f2}	5.5	g_2	0.75	W_3	7

Table 2.2: PIN diode states and frequency reconfigurable antenna (ANT2) band of operations.

States	PIN Diode (ON/OFF)	Frequency Band (GHz) (Simulated)
State_1	ON	4.3 GHz - 5.5 GHz
State_2	OFF	5.1 GHz - 6.8 GHz

2.2.2 Ground Plane and T-Shaped Stub Design for Isolation Enhancement

The performance of the proposed antenna depends significantly on the ground plane. This ground plane provides impedance matching and enhances isolation between antenna elements. Ground1 has dimensions of ($W \times L_g$) mm^2. The inclusion of a stub with ($L_1 \times W_2$) mm^2 on the ground plane forms Ground2. Further, a stub of ($L_2 \times (2\ W_3 + W_2)$) mm^2 is employed to form a T-shaped stub ground plane as Ground3. Figure 2.2 depicts the design evolution of the ground plane.

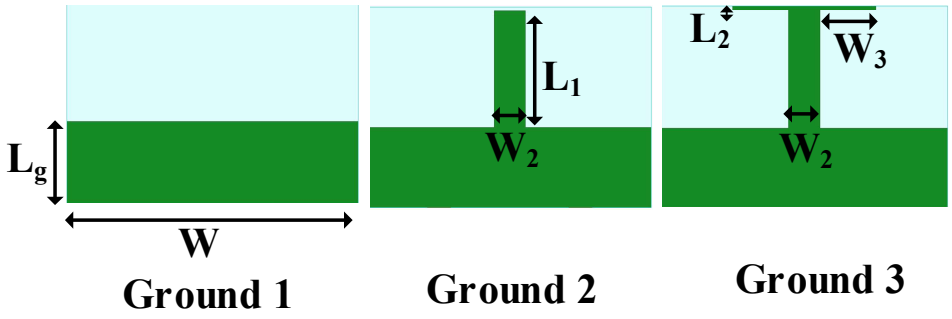

Figure 2.2: Ground plane geometry evolution.

The requirement of a lower cut-off frequency (f_c) for a UWB antenna is 3.1 GHz. With Ground1, the lowest f_c of the UWB antenna (ANT1) is 4.2 GHz. Since this frequency does not satisfy the requirement of UWB, a stub is added to Ground1, which shifts the f_c of the UWB antenna (ANT1) to 3.1 GHz for Ground2 [62, 86]. In Ground3, one more stub is added to form a T-shaped stub. It is observed that further shifts in the lower cutoff frequency to 2.7 GHz. Cognitive radios use this frequency range for scanning.

Ground3 also improves the isolation between ports. The effect of the ground plane on the UWB antenna (ANT1) reflection coefficient is depicted in Figure 2.3. Figure 2.4 (a) and (b) illustrate the ground plane effect on the frequency reconfigurable antenna (ANT2). In Figure 2.4 (a), State_1, when the diode is ON, the lowest cut-off frequency is shifted lower to 4.3 GHz with the modification of the ground plane. In Figure 2.4(b), State_2, when the diode is OFF, the lowest cut-off frequency observed is 5.1 GHz.

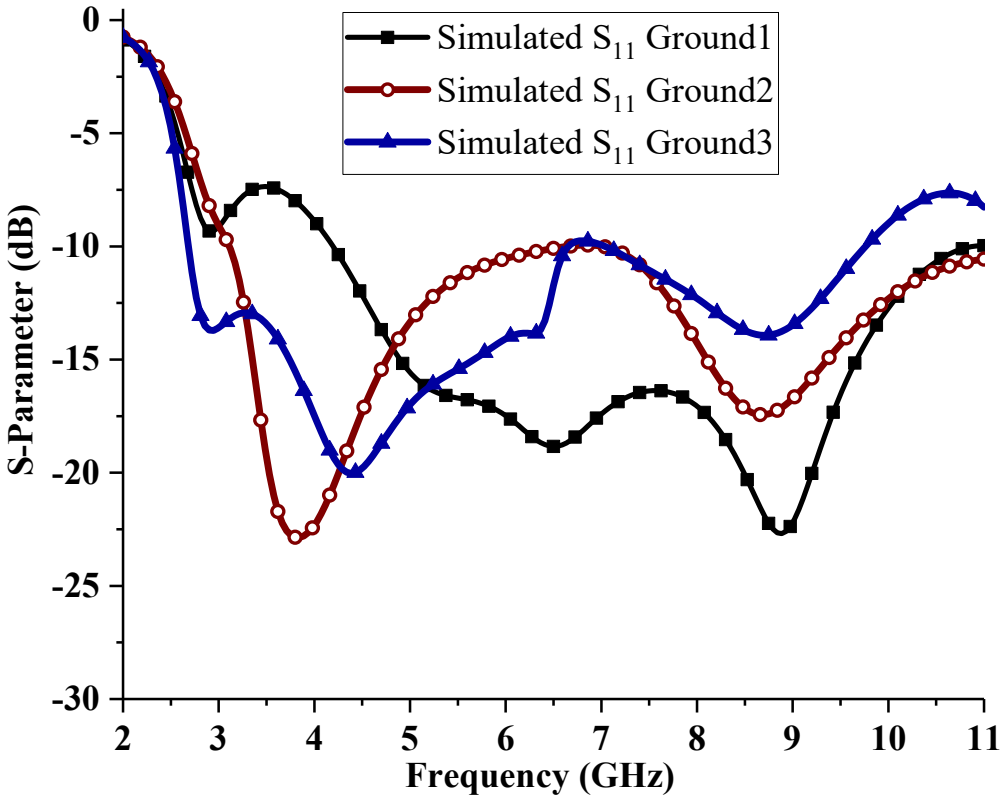

Figure 2.3: Ground plane effect on UWB antenna (ANT1) reflection coefficient (S_{11}).

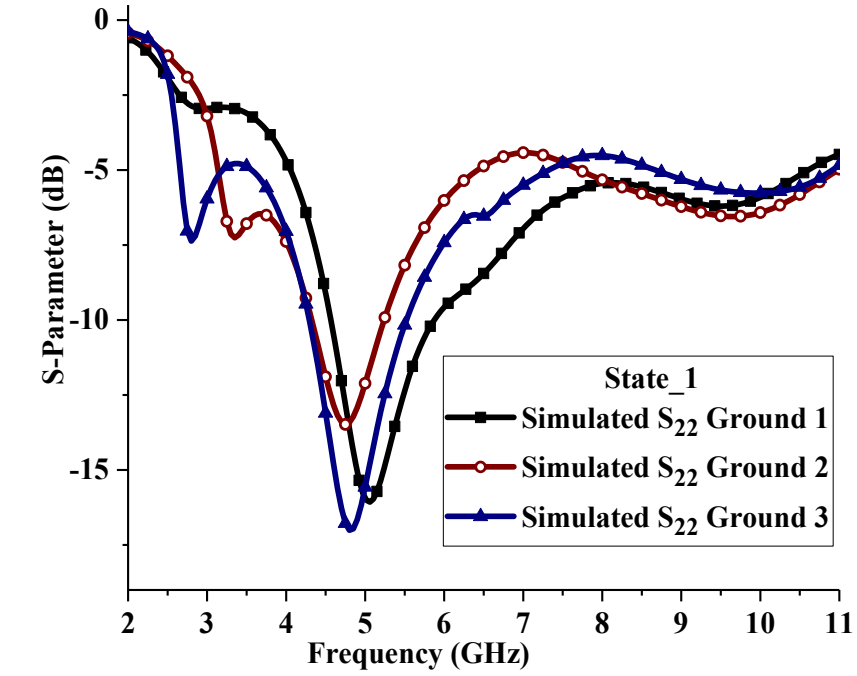

(a)

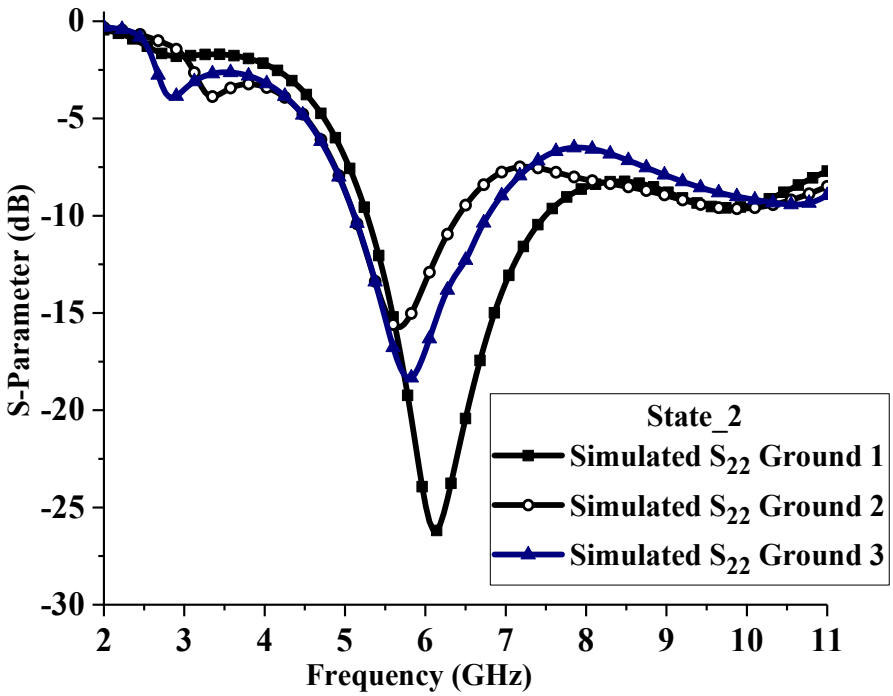

(b)

Figure 2.4: Ground plane effects on ANT2 reflection coefficient (S_{22}) in (a) State_1, (b) State_2.

The ground plane effect for the isolation (S_{12}) enhancement between antennas elements within the operating frequency range of the communicating antenna (ANT2) is shown in Figure 2.5(a) and 2.5(b).

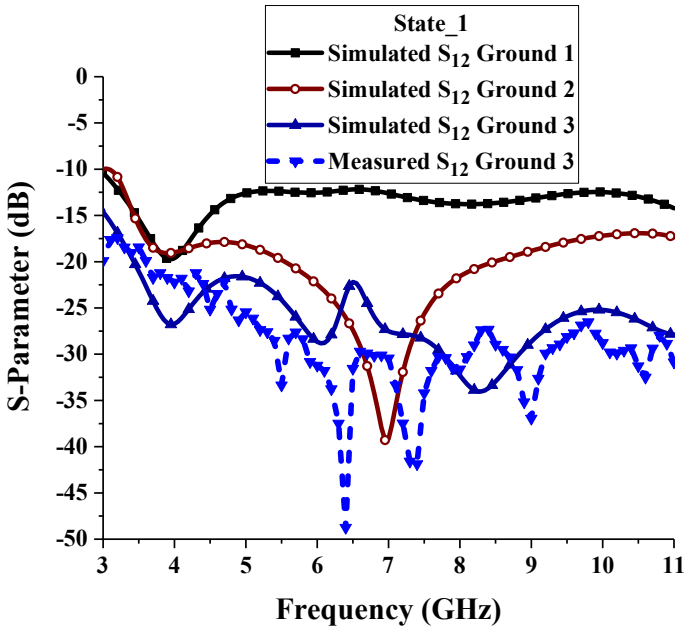

(a)

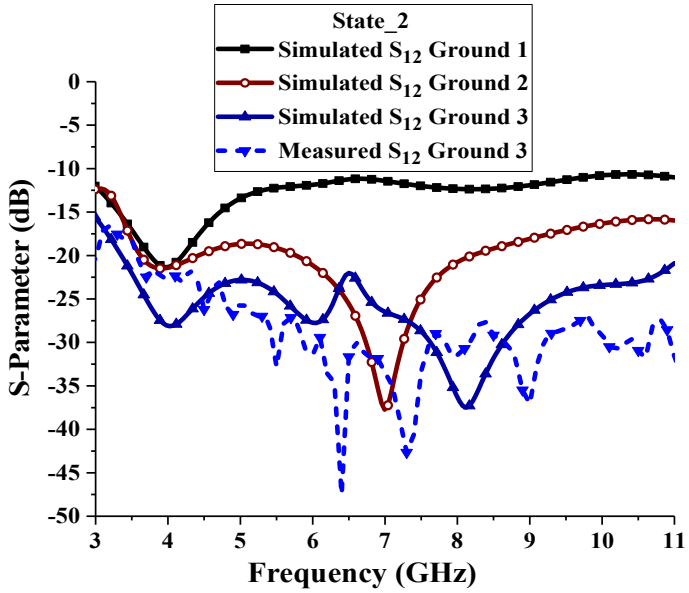

(b)

Figure 2.5 (a): Simulated and measured S-parameter (S_{12}) for various ground plane configurations in State_1. (b) State_2.

From the Figure 2.5(a), in the case of Ground1, it is observed that the isolation (S_{12}) between ANT1 and ANT2 is very poor (11 dB) in the operating frequency range of communicating antenna (ANT2). The inclusion of a stub with ($L_1 \times W_2$) mm^2 on Ground2 reduces the mutual coupling up to -19 dB because of the change in surface current distribution on the ground plane. Furthermore, in Ground3, a T- shaped stub is employed to further decreases mutual coupling (S_{12}) to -21 dB over the frequency reconfigurable antenna operating range in State_1 (4.3 GHz − 5.5 GHz) and State_2 (5.1 GHz − 6.8 GHz).

2.3. Results and Discussion

The proposed antenna is simulated using the EM full-wave simulator HFSS version 22.2 [109]. The MITS-eleven Lab prototyping machine is used to create a prototype of the antenna. The PIN diode biasing is done with a DC biasing voltage and wires soldered on the DC pad. VNA Master MS2038C is used to measure and validate the simulated results obtained from the proposed antenna. The fabricated prototype of the proposed antenna is shown in Figure 2.6 (a) and (b).

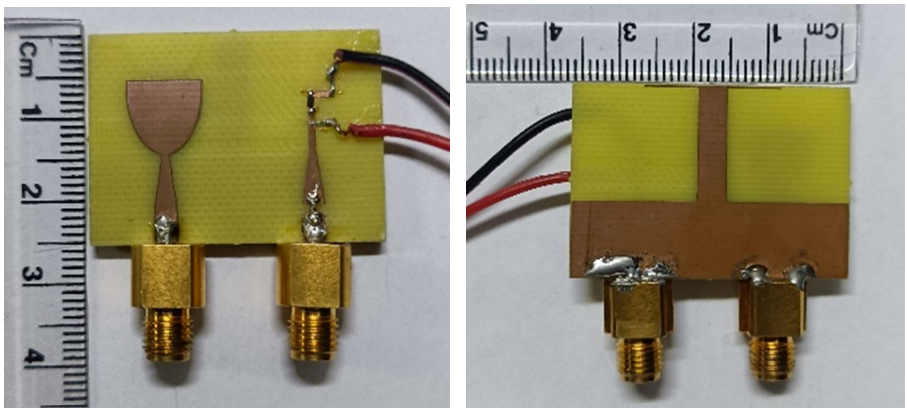

(a) Top View (b) Bottom view

Figure 2.6: Fabricated prototype of proposed antenna.

2.3.1. Reflection Coefficient Measurement

The simulated and measured reflection coefficient (S_{11}) for ANT1 and (S_{22}) for ANT2 with two states are shown in Figure 2.7, Figure 2.8(a) and 2.8(b), respectively. The measured impedance bandwidth (S_{11} < -10 dB) for the UWB antenna (ANT1) is 8.5 GHz (2.5 GHz to 11 GHz). While performing the S_{11} measurement of ANT1, ANT2 is terminated with 50 Ω matched load. Similarly, while measuring the S_{22} of ANT2, the ANT1 port is terminated with a matched load of 50 Ω. The measurement result shows close agreement with the simulated result for most of the frequency bands, as shown in Figure 2.7. Due to manufacturing and measurement tolerances, a small disparity between simulated and measured values is seen [79].

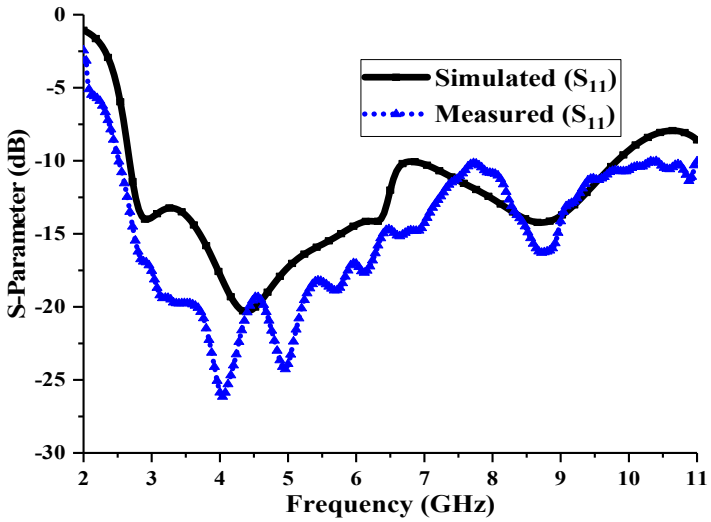

Figure 2.7: Simulated and measured reflection coefficient (S_{11}) of the UWB antenna (ANT1).

Figure 2.8 (a) compares the simulated and measured reflection coefficient (S_{22}) of the reconfigurable antenna (ANT2) for State_1. The PIN diode is ON in this state_1, and the measured impedance bandwidth (S_{22} < -10 dB) is 2.08 GHz (4.32 to 6.4 GHz).

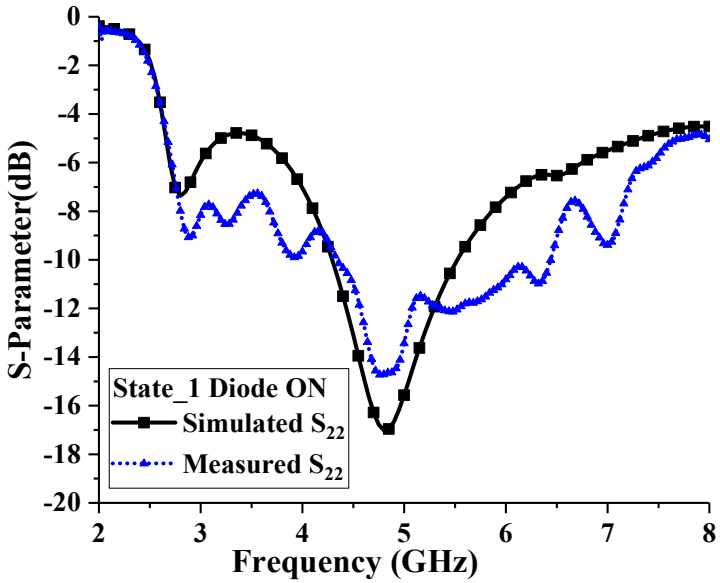

(a)

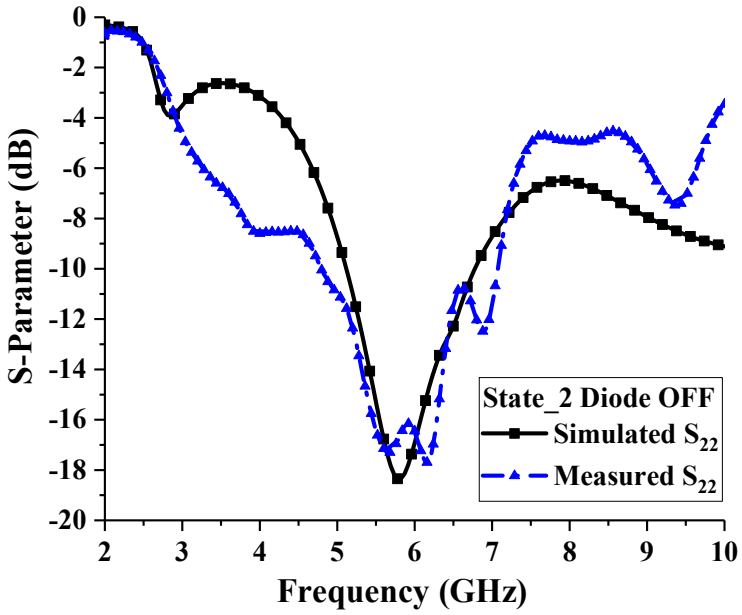

(b)

Figure 2.8: Simulated and measured reflection coefficient of reconfigurable antenna in (a) State_1 (Diode ON), (b) State_2 (Diode OFF).

Figure 2.8(b) depicts simulated and measured reflection coefficient (S_{22}) of reconfigurable antenna for State_2. The PIN diode is OFF in State_2. The measured impedance bandwidth (S_{22} < -10 dB) for State_2 is 2.36 GHz (4.74 GHz to 7.1 GHz).

In both cases (State_1 and State_2), the measured impedance bandwidth is wider than the simulated bandwidth. It is caused by fabrication tolerances, losses due to the SMA connector and uncertainty in loss tangent of substrate [79, 86, 104]. Isolation (S_{21}) between ANT1 and ANT2 is given by Figure 2.9. This confirms very less mutual coupling of -21 dB, between two antennas over the communication antenna (ANT2) operating range.

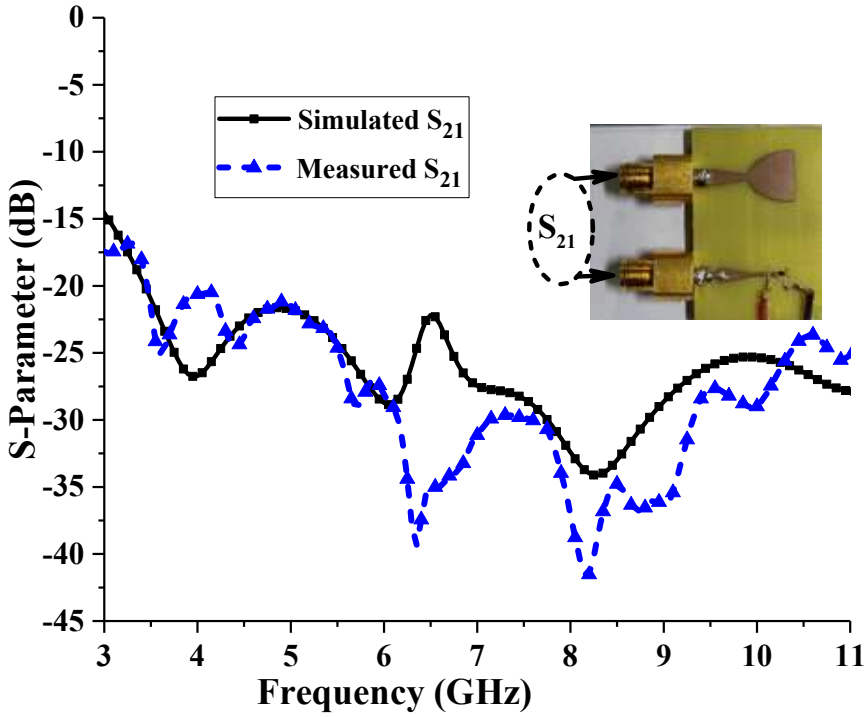

Figure 2.9: Simulated and measured S-parameter (S_{21}) (diode OFF, State_2).

2.3.2. Radiation Patterns and Gain

Figure 2.10 shows the fabricated prototype of antenna inside anechoic chamber. At the transmitting end, a broadband horn antenna (1–18 GHz) is used. The proposed antenna is in far field at receiving end.

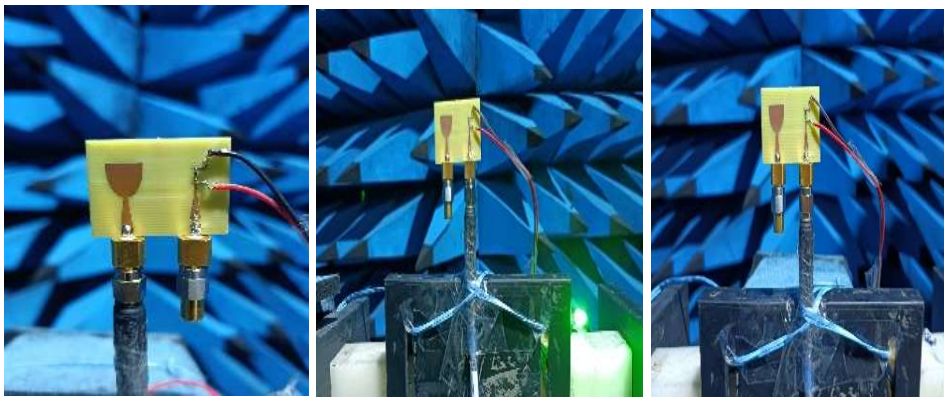

(a) (b) (c)

Figure 2.10: Fabricated prototype antenna in an anechoic chamber (a) ANT1 (UWB) and ANT2 (b) State_1, (c) State_2.

The radiation patterns are measured at several representative frequencies, such as 3.0 GHz, 6.8 GHz, and 8.6 GHz, within the UWB range. These measurements are taken when Port1 (ANT1) is excited and Port2 is matched with 50 Ω. Figure 2.11(a) and 2.11(b) show the simulated and measured normalized radiation patterns of ANT1 in (x-z) E-plane and (y-z) H-plane, respectively.

It can be seen that in the E-plane, the antenna exhibits a dumbbell-shaped pattern at lower frequencies, but at higher frequencies, the pattern is more omnidirectional because of the current distribution in the T-shaped stub [86]. While in (y-z) H-plane, the antenna exhibits a dumbbell-shaped pattern at lower frequency at 3.0 GHz, and a nearly omnidirectional radiation pattern is observed for ANT1 at frequencies 6.8 GHz and 8.6 GHz. The cross-polarization level is below than 15 dB in both x-z and y-z planes.

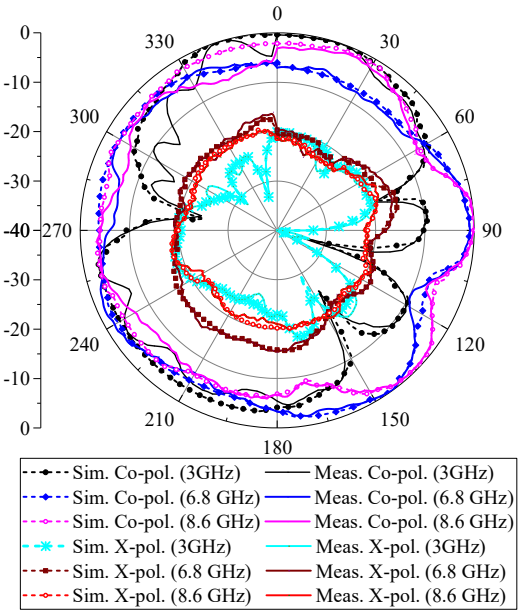

(a)

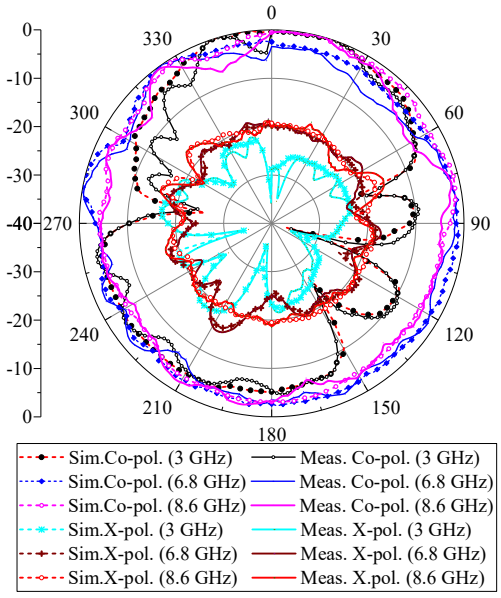

Figure 2.11: Simulated and measured normalized radiation patterns for ANT1 (UWB) (a) E-Plane, (b) H-Plane at 3.0 GHz, 6.8 GHz, and 8.6 GHz.

The radiation pattern for ANT2 is measured for State_1 and State_2 at frequencies 4.8 GHz and 5.9 GHz, respectively. These measurements are taken when Port2 (ANT2) is excited and Port1 is matched with 50 Ω. Figure 2.12(a), depicts the simulated and measured radiation patterns in E- and H-plane for State_1 (Diode ON), and Figure

2.12(b) depicts the measured radiation patterns in E- and H-plane for State_2 (Diode OFF). From Figure 2.12(a), it is observed that the E-plane radiation patterns are more directional, which is caused by the isolating stub and current distribution in ANT2, while in the H-plane (y-z), omnidirectional patterns have been observed.

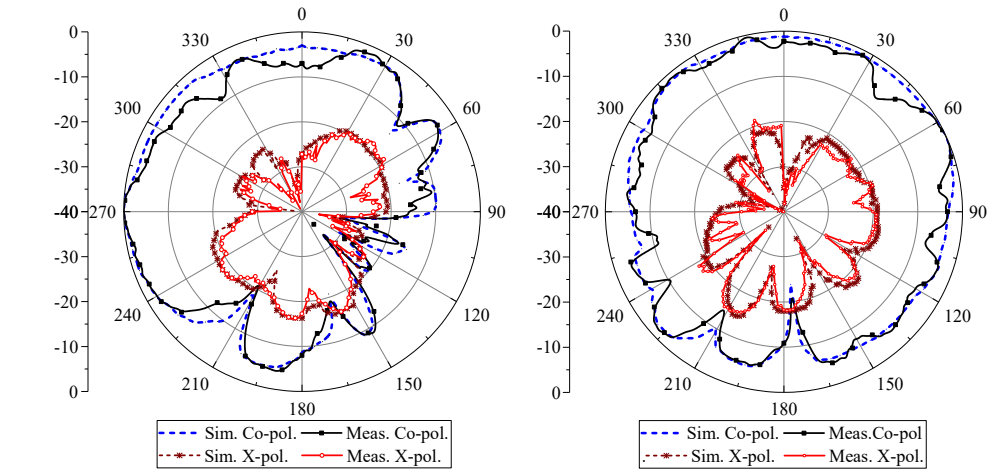

(a)

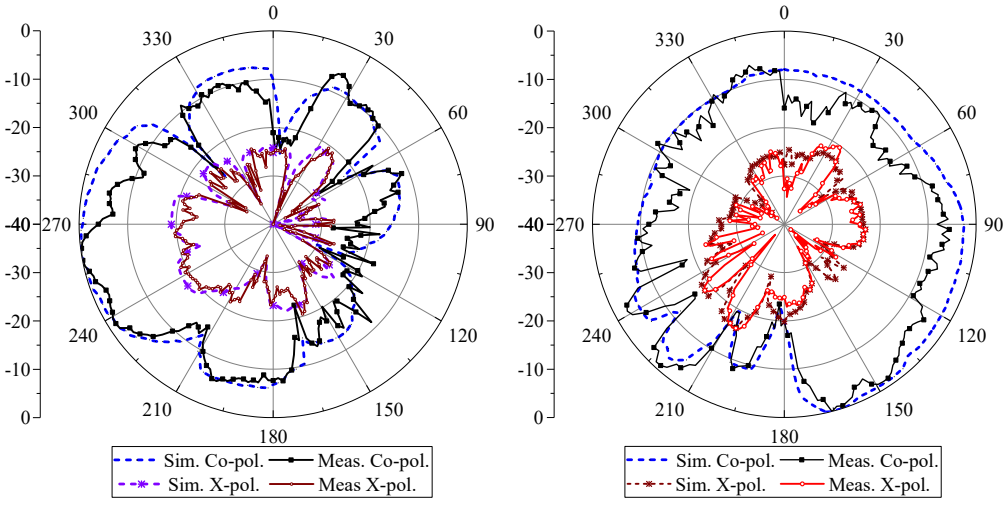

(b)

Figure 2.12: Simulated and measured normalized radiation pattern for ANT2, (a) State_1 at 4.8 GHz E- and H-Plane and (b) State_2 at 5.9 GHz, E-Plane and H-Plane.

In Figure 2.12(b) (State_2), when the diode is OFF, the measured radiation patterns in E-Plane are skewed in one direction, and H-Plane shows a nearly omnidirectional pattern. The pattern's asymmetry is due to the isolating stub, resulting in a slightly

directional radiation pattern. It is observed that the cross polarization for ANT2 in State_1 and State_2 is below than 15 dB in both x-z and y-z planes.

Figure 2.13(a) shows the simulated and measured realized gain of ANT1. ANT1 exhibits a positive gain over the UWB frequency range (2.7 GHz to 10 GHz).

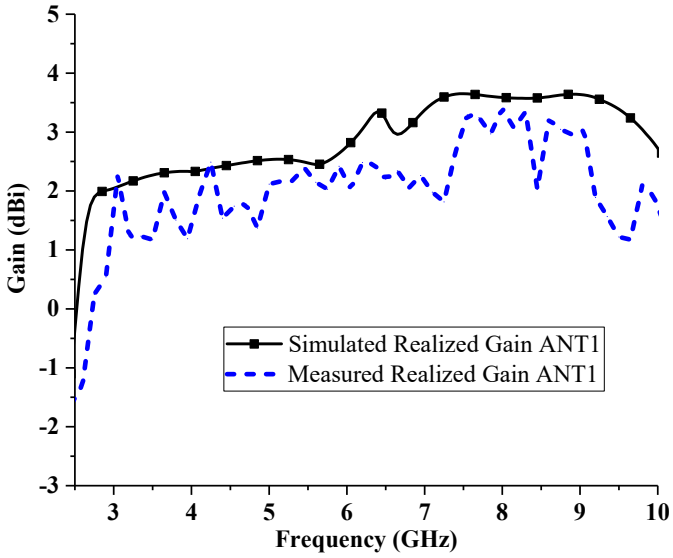

(a)

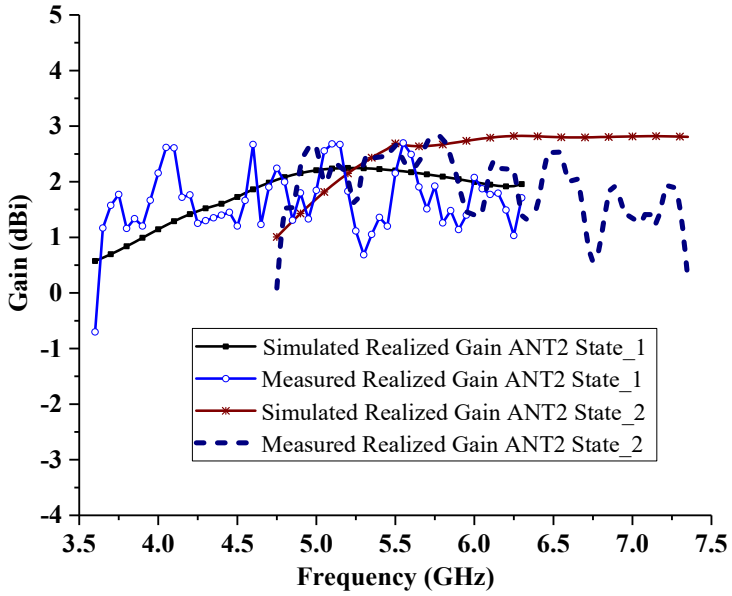

(b)

Figure 2.13: Realized gain of the proposed antenna (a) ANT1, (b) ANT2 (State_1 and State_2).

ANT2 also exhibits a positive gain over the frequency range of communication in State_1 and State_2. Simulated and measured realized gains for ANT1 and ANT2 are in good agreement and depicted in Figure 2.13 (a) and 2.13(b).

2.3.3. Surface Current Distribution

To better understand the isolation between Port1 and Port2 of the proposed antenna, the distribution of surface current on different antenna configurations with different ground planes is depicted in Figure 2.14. Figure 2.14 (a), (b), and (c) represent the Ground1 configuration. Figure 2.14 (d), (e), (f), and Figure 2.14 (g), (h), (i) represent Ground2 and Ground3 configurations, respectively. Figure 2.14 (a), (d), (g) shows that Port1 (ANT1) is excited, and the distribution of surface current at 4.8 GHz is depicted, where the S_{21} values are relatively higher for the ANT1 within the range of the ANT2 communication range. This frequency is also the resonance frequency of ANT2 in State_1. Figure 2.14 (b), (e), and (h) represents that Port2 (ANT2) is excited, and the surface current distribution is plotted for the 4.8 GHz. Similarly, Figure 2.14 (c), (f), and (i) represent the surface current distribution for Port2 (ANT2) in State_2 at a frequency of 5.9 GHz. For Ground1, it is clearly observed that a high level of surface current is found near Port1 and Port2 when Port2 and Port1 are excited, respectively. This shows the isolation between ports is very poor in the case of Ground1. A stub is added to the ground plane between ANT1 and ANT2 to minimize this mutual coupling. It is observed from the investigation that the isolation between ports is enhanced at the ANT2 State_2 frequency band. Still, the isolation is not much improved at the lower frequency band where the communication antenna (ANT1) operates in State_1. From Figure 2.14 (d), (e), (f), it is observed that the surface current is more confined to the excited antennas and towards the extended stub. Therefore, the mutual coupling is

reduced between antenna ports. One more stub is added to the previous stub to form a T-shaped stub to enhance the isolation further at ANT1 State_1 frequency. It is noticeable in Ground3, this extension of stub provides the increased path length to the surface current, which provides a good mutual coupling of -21 dB between antennas at State_1 of ANT2. The mutual coupling between antennas in State_2 is also well below -21 dB.

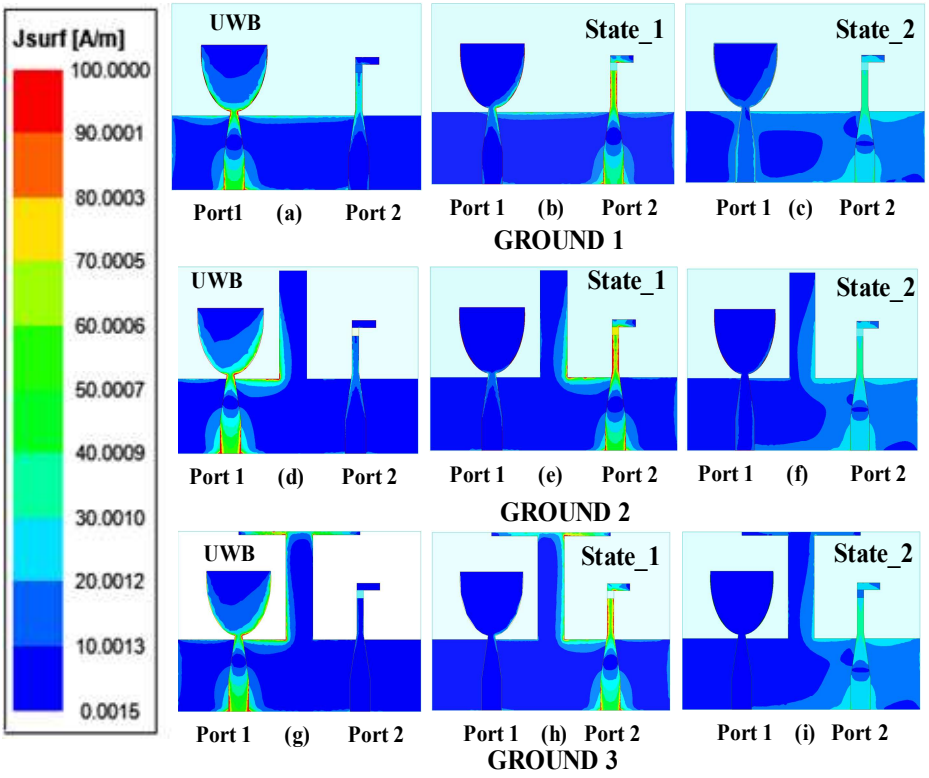

Figure 2.14: Simulated surface current density of proposed antenna in different cases of the ground plane and two states of PIN diode (State_1) and (State_2).

2.3.4. Diversity Performance

The envelope correlation coefficient (ECC) evaluates the level of correlation between antenna elements. The mutual coupling effect between ports (antenna elements) can be approximated using scattering parameters.

Diversity gain (DG) refers to the improvement in signal-to-noise ratio due to the use of diversity. The ECC and DG by using the S-parameters of the proposed antenna are estimated and depicted in Figure 2.15 and Figure 2.16, respectively. The ECC and DG are related. The lower ECC values correspond to higher DG.

The ECC and DG are calculated by [56, 87,110, 111].

$$\mathrm{ECC} = \frac{|\, S_{11}^{*} S_{12} + S_{21}^{*} S_{22} \,|^{2}}{(1-(|\, S_{11} \,|^{2} + |\, S_{21} \,|^{2}))(1-(|\, S_{22} \,|^{2} + |\, S_{12} \,|^{2}))} \tag{2.1}$$

$$\mathrm{DG} = 10\sqrt{1 - |\mathrm{ECC}|^{2}} \tag{2.2}$$

Figure 2.15, shows the ECC plot versus frequency for ANT1 and ANT2. The ECC must be less than 0.5 (<0.5) for better diversity performance of the antenna. However, the ideal value of ECC is zero (ECC = 0). The measured ECC is less than 0.05 all over the UWB band for ANT1 and less than 0.035 for ANT2 for State_1 and State_2. Moreover, the value of ECC is less than 0.03 for ANT1 within the range of ANT2.

Figure 2.16 shows the DG plot versus frequency for ANT1 and ANT2. The diversity gain ideal value is 10 dB.

The simulated and measured DG for ANT1 is 9.9 dB throughout the UWB band. Similarly, for ANT2, it is 9.9 dB over the operating range in State_1 and State_2. This indicates good diversity performance of the proposed antenna.

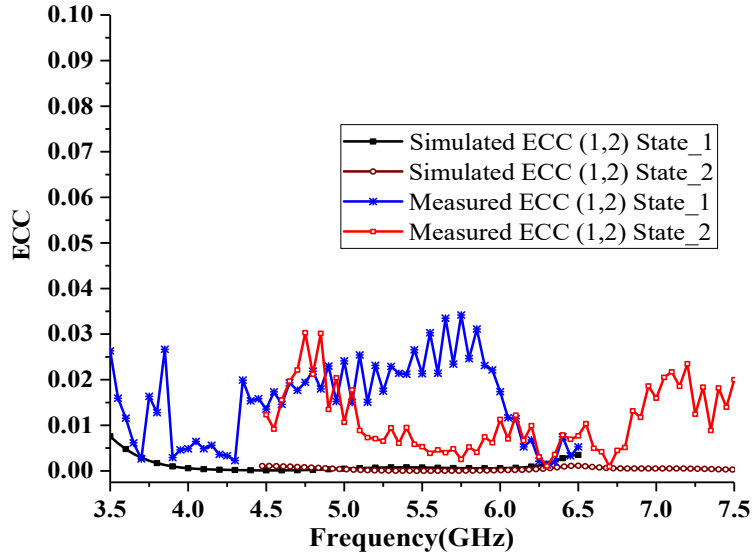

Figure 2.15: Simulated and measured ECC

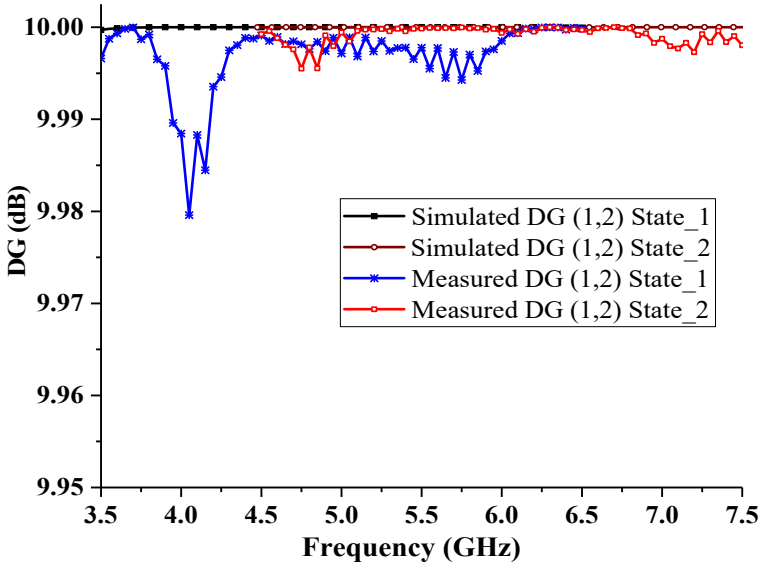

Figure 2.16: Simulated and measured Diversity Gain (DG)

Table 2.3: Performance comparison of the proposed antenna and other reported antenna

Ref.	Type (UWB/ CR/ Dual-band)	Size (in terms of λ_g)*	Isolation Enhancement Technique	Bandwidth (GHz)	Mutual coupling (dB)	Ground
[51]	CR	$0.54\lambda_g \times 0.54\ \lambda_g \times 0.01\ \lambda_g$	Multiple EBG and isolation stub	Ant1 (2 -11) Ant2 (4.63 - 6.42)	-25 dB	Common
[79]	CR	$0.71\lambda_g \times 0.78\ \lambda_g \times 0.01\ \lambda_g$	-	Ant1 (3.1-10.6) Ant2 (4.9-5.35)	-4 to -10 dB	Common
[86]	UWB	$0.28\lambda_g \times 0.46\ \lambda_g \times 0.02\ \lambda_g$	L-shape, I-shape stub	(3.1– 10.6)	-15 dB	Common
[100]	CR	$0.6\lambda_g \times 1\ \lambda_g \times 0.02\ \lambda_g$	-	Ant1 (3.1 - 10.6) Ant2 (3.3-6.3)	-15 dB	Isolated ground
[102]	Dual Band	$0.96\lambda_g \times 0.66\ \lambda_g \times 0.02\ \lambda_g$	DGS, Parasitic Stub	3.409-3.601 4.76-5.04	-22.3 dB -30.8 dB	Common
[103]	CR	$0.41\lambda_g \times 0.41\ \lambda_g \times 0.01\ \lambda_g$	CSRR, DCRR and Parasitic meander line	1.9 -11.77	-22 dB	Isolated ground
This work	CR	$0.36\lambda_g \times 0.53\ \lambda_g \times 0.02\ \lambda_g$	T-shaped stub	Ant1 (2.7 - 10) Ant2 State_1 (4.3 - 5.5) Ant2 State_2 (5.1 - 6.8)	-21 dB	Common

*λ_g is the guided wavelength at lowest operating frequency.

The comparison on the basis of size, isolation technique, bandwidth and isolation between ports of the proposed antenna with previously reported antennas for CR, UWB and dual band is presented in Table 2.3.

The isolation in [51, 102] is comparatively good but has a larger antenna aperture and encompasses multiple isolation techniques. However, our proposed antenna is compact and provides less mutual coupling of -21 dB over the ANT1 and ANT2 operating range. As per the author's knowledge, this work is unique, which integrates compact UWB (ANT1) and frequency reconfigurable antenna (ANT2) sharing common ground and with high isolation over the two bands of operation of ANT2 in cognitive radio.

2.4 Summary

An integrated compact UWB and frequency reconfigurable antenna with high isolation for cognitive radio have been proposed in this chapter. The simulation and experimental studies of the proposed antenna have been done. The reflection coefficients versus frequency and isolation between antenna ports, radiation patterns, surface current distribution, and realized gain have been reported. T-Shaped stub in ground plane improves the isolation with mutual coupling less than -21 dB. The impedance bandwidth of 7.3 GHz (2.7 GHz to 10 GHz) for the UWB antenna and the impedance bandwidth of 1.2 GHz for ANT2 in State_1 and 1.7 GHz for ANT2 in State_2 have been attained. The proposed compact antenna is a potential candidate for interweave cognitive radio applications.